Energetic Ion Bombardment of Ag Surfaces by C_{60}^+ and Ga^+ Projectiles

Shixin Sun, Christopher Szakal, and Nicholas Winograd
Department of Chemistry, The Pennsylvania State University, University Park, Pennsylvania, USA

Andreas Wucher
Physics Department, University of Duisburg-Essen, Essen, Germany

The ion bombardment-induced release of particles from a metal surface is investigated using energetic fullerene cluster ions as projectiles. The total sputter yield as well as partial yields of neutral and charged monomers and clusters leaving the surface are measured and compared with corresponding data obtained with atomic projectile ions of similar impact kinetic energy. It is found that all yields are enhanced by about one order of magnitude under bombardment with the C_{60}^+ cluster projectiles compared with Ga^+ ions. In contrast, the electronic excitation processes determining the secondary ion formation probability are unaffected. The kinetic energy spectra of sputtered particles exhibit characteristic differences which reflect the largely different nature of the sputtering process for both types of projectiles. In particular, it is found that under C_{60}^+ impact (1) the energy spectrum of sputtered atoms peaks at significantly lower kinetic energies than for Ga^+ bombardment and (2) the velocity spectra of monomers and dimers are virtually identical, a finding which is in pronounced contrast to all published data obtained for atomic projectiles. The experimental findings are in reasonable agreement with recent molecular dynamics simulations.   (J Am Soc Mass Spectrom 2005, 16, 1677–1686) © 2005 American Society for Mass Spectrometry

T he elucidation of the mechanism of interaction of energetic polyatomic or cluster ions with surfaces is of current interest since these projectiles are now being extensively employed as desorption probes in secondary ion mass spectrometry (SIMS) experiments [1, 2]. Because of their propensity to produce higher molecular ion signals than corresponding atomic ions and the emergence of commercially available C_{60}^+ [3, 4] and Au_3^+ [5, 6] ion guns, applications have expanded dramatically. For example, these sources can be focused onto the sample with a probe size about 1 micron, allowing greatly improved molecule-specific imaging experiments. The high secondary ion yield associated with the cluster/solid interaction also allows for molecular depth profiling studies without the accompanying damage accumulation normally associated with atomic bombardment [7–17].

The mechanisms associated with the observed secondary ion yield enhancement are not yet clear, although details are emerging quickly. A basic question that must be resolved is to determine whether the yield enhancement occurs as a consequence of increased ionization efficiency, or is due to more effective sputtering in the neutral desorption channel. There is mixed

information about this point. For In and Ag surfaces, for example, it has been shown that the enhanced secondary ion yield under SF_m^+ bombardment ($m = 1$–5) largely arises from the enhanced ionization efficiency attributable to implanted F atoms [18]. For organic systems, however, very high removal rates of neutral species have been reported [2], obviating the need to invoke enhancement of the secondary ionization probability. Most recently, yields and velocity distributions were measured for In and In_2 sputtered from In surfaces bombarded with Au^+, Au_2^+, and Au_3^+ [19]. Although these experiments do not address the issue of enhanced ionization, they do show that there are enhancements in the sputtering yield that cannot be explained by either collision cascade theory or by thermal spikes. The spike model has traditionally been employed to interpret the response of metallic targets to cluster bombardment [20]. Instead, the emission mechanism is proposed to involve the quasi-free expansion of a super-critically heated subsurface volume.

Recent molecular dynamics (MD) computer simulations show a largely different desorption process for isoenergetic Ga and C_{60} bombardment [21, 22]. For 15 keV Ga bombardment of Ag{111}, atomic motion is described by a classic collision cascade with a desorption yield of about 20 Ag atoms per incident Ga^+ ion. For 15 keV C_{60} bombardment, however, crater formation with minimal subsurface damage has been reported and there is virtually no evidence for the forma-

tion of traditional collision cascades. The desorption yield of Ag is predicted about 300 atoms per C_{60} impact, suggesting an enhancement factor of about 15-fold. Even larger enhancements are observed for small sputtered clusters of Ag. These recent calculations of neutral C_{60} bombardment produce results consistent with earlier MD calculations for the C_{60} bombardment of graphite [23–25]. Crater formation has also been observed using other systems as well [24–27]. None of these calculations addresses the issue of enhancements in the ionization channel, of course, but they do provide basic information about how the atoms move under these novel circumstances.

In this paper, we expand upon earlier experiments comparing the bombardment of Ag{111} with energetic Ga^+ and C_{60}^+ projectiles to make direct comparisons with the published MD calculations. The results show that the enhanced secondary ion yields observed for this system are predominantly caused by enhancements of the respective partial sputter yields, as measured by quartz crystal microbalance (QCM) experiments. More specifically, we find that the neutral Ag yield is increased about 6-fold under bombardment with 15-kev C_{60}^+ compared with isoenergetic Ga^+ projectiles. For sputtered neutral Ag_2 and Ag_3, the yield enhancements are even larger, in qualitative agreement with the calculations. Moreover, velocity distributions of neutral atoms and clusters are found to exhibit pronounced differences between Ga^+ and C_{60}^+ bombardment. These results also agree with the predictions of the MD calculations and further support the recently proposed notion that cluster bombardment produces a response that is reminiscent of a quasi-free expansion of desorbing particles.

Experimental

Experiments were performed using a TOF-SIMS instrument, which has been described in detail previously [28]. The instrument is equipped with two ion sources to generate the primary ion beams employed here. A standard liquid metal ion source (Ionoptika Ltd., Southhampton, United Kingdom) delivers Ga^+ ions with kinetic energies up to 25 keV. Although the beam is in principle focusable to diameters below 100 nm, it is operated here at a spot size of about 1 μm, resulting in a total ion current of several nA.

The second source is designed to produce buckminsterfullerene (C_{60}) cluster ions with kinetic energies up to 20 keV [3, 4]. To generate the C_{60}^+ cluster ions, buckminsterfullerene powder (Aldrich, Milwaukee, WI) is evaporated at about 400 °C, and the resulting C_{60} vapor is ionized by electron impact. The subsequent ion beam consists mainly of singly and doubly charged C_{60} ions, the relative contributions of which can be controlled by means of the electron impact energy. In the experiments performed here, the source is operated with a relatively low electron impact energy of 30 eV which was shown to produce a relatively pure C_{60}^+ beam

[29]. Under the selected operation conditions, the source delivers a total ion current of about 1 nA into an irradiated spot of about 30 μm diameter.

TOF Spectrometer

Both ion beams are carefully overlapped, and either the Ga^+ or the C_{60}^+ ions are used to bombard the investigated surface to release secondary ions and neutral particles. The primary ion bombardment is operated in a pulsed mode with pulse durations ranging from about 1 μs down to 50 ns. During the primary ion pulse, the sample is kept at ground potential to ensure that the impinging beam is not deflected by the ion extraction field.

While the secondary ions are directly accessible to mass analysis, the sputtered neutral particles are intercepted by a pulsed laser beam for postionization. Both secondary ions and photoions are then extracted into a time-of-flight (TOF) mass analyzer by applying a pulsed positive potential of 2.5 kV to the sample stage. The extraction pulse was delayed with respect to the end of the primary ion pulse by a variable time which will in the following be called "stage delay." For postionization experiments, the ionizing laser beam is guided parallel to the sample surface at a distance of ~1 mm. The firing time of the laser pulse is delayed with respect to the ion extraction pulse by a variable time interval ("laser delay").

The Ti:Sapphire femtosecond laser system (Clark-MXR, Inc., Dexter, MI) employed here has been described elsewhere [30, 31]. The system is based on an Ar ion laser-pumped, self-mode-locked Ti:Sapphire oscillator that generates 800 nm pulses with 50 fs pulse width and 300 nJ/pulse energy. The pulses go through two stages of amplification to reach a final output of up to 3.5 mJ/pulse at a wavelength of 800 nm and a repetition rate of 1 kHz. The laser beam is coupled to the vacuum chamber via a CaF_2 lens with 25 cm focal length. The focal conditions are chosen such as to produce a beam cross section of 150 μm diameter in the interaction region above the sample surface.

During the measurements determining the partial sputtering yield of sputtered atoms and clusters, a relatively long projectile ion pulse of about 1 μs duration is chosen. This ensures that particles of all relevant emission velocities are present in the ionization volume and interact with the ionizing laser. To determine the emission velocity distributions of sputtered neutral particles, on the other hand, the primary ion pulse width is reduced to 100 ns, and a controlled time delay between the projectile ion and the ionizing laser pulse is introduced as the sum of stage and laser delay. This operation mode selects the emission velocity of the detected neutral particles via their flight time between the surface and the ionization volume.

The velocity distribution $f(v)$ of the sputtered neutrals is evaluated from the measured delay time distribution $s(t)$ of the detected photoion signals by [32],

$$f(v) \propto \frac{s(t) \cdot t}{\Delta r + r/t \, \Delta t} \tag{1}$$

where r denotes the distance between the sample surface and the laser ionization volume, Δr is the spatial extension of the laser beam in the direction along the surface normal (570 μm) and Δt is the laser pulse width. Due to the ultrashort laser pulse duration of about 100 fs, the second term in the dominator of eq 1 is far smaller than the first term and may safely be omitted. The emission velocity v is given by r/t, requiring an accurate measurement of r. This is done by translating the laser beam towards the sample surface until ablation occurs, indicated by large corresponding ion signals shown in the spectrum.

The mass selected ions are detected by means of a Chevron stack of two microchannel plates (MCP) that are operated with 18 keV postacceleration. During registration of neutral atoms and small clusters, a flight time peak may be composed of many ions, and therefore, an analog detection scheme is employed in which the charge produced by the MCP is directly digitized by means of a fast transient recorder. To avoid detector saturation, the gain voltage across the MCP is reduced such as to ensure that the maximum recorded signal does not exceed a height of about 100 mV at 50 Ohm termination.

The Ag sample used for measuring postionized neutrals was purchased from Aldrich. A small piece of polycrystalline silver foil is etched for 30 s in 30% HNO_3, then rinsed with water and methanol and dried with N_2. After introduction into the UHV system (base pressure 1×10^{-9} mbar), the surface is sputter-cleaned using C_{60}^+ ion bombardment until all peaks in the mass spectra reach a steady-state value, usually after an ion fluence of 10^{15}–10^{16} cm^{-2}.

Quartz Crystal Microbalance

The total yield of Ag is measured using a quartz crystal microbalance (QCM, Maxtek TM-400, Cypress, CA). For that purpose, a standard AT-cut quartz crystal with a resonance frequency of 6 MHz is mounted in a specially modified sample holder. The crystal is coated with a finely polished Au top contact electrode which covers the entire crystal area of 13 mm diameter. The bottom electrode has a smaller diameter of 6.6 mm. A polycrystalline Ag layer of about 500 nm thickness is vapor-deposited onto the top electrode, forming the target surface for the ion bombardment experiments. A Cr barrier layer of 50 nm thickness was introduced between the Ag and Au films to prevent the formation of an Ag-Au alloy. Upon introduction into the UHV system, a stable situation is reached within a few minutes with a displayed deposition rate of zero. If the dc ion bombardment is switched on, a negative deposition rate is displayed, indicating the sputter removal of surface material. The removal rate is measured by

integrating the total thickness variation displayed by the controller over a time period of 60 s (C_{60}) or 300 s (Ga). To ensure that the measured data is not influenced by thermal drift, it is verified that the displayed removal rate value returns to zero after the ion bombardment is switched off.

For a homogeneous deposition or removal of an aerial mass density Δm_a (g/cm^2) at the top electrode of the quartz, the frequency change Δf is described by [33]

$$\Delta m_a = D_\infty \cdot \Delta f, \tag{2}$$

provided the total change is sufficiently small (<2% [34] compared with the nominal resonance frequency f (6 MHz).

The QCM controller used here has been designed as a film thickness monitor and therefore displays a thickness change Δd (nm) instead of the frequency change. Apart from a minor correction for differences in the acoustic impedance of quartz and coating material (which is only important for large frequency changes and therefore always negligible in our experiments), the displayed value of Δd is internally calculated as

$$\Delta d = F_t \cdot \frac{\rho_q}{\rho_f} \cdot N_q \cdot \Delta\tau, \tag{3}$$

where ρ_q denotes the density of the quartz, $N_q = 1.668 \times 10^5$ (Hz·cm) is the quartz constant permanently programmed into the controller, and $\Delta\tau$ is the measured change of the quartz oscillation period $\tau = 1/f$. To correct for the density ρ_f of the coating film, an assumed value is input into the controller by the user. The displayed values of Δd were corrected for the user selectable tooling factor F_t to correspond to $F_t = 1$.

From eqs 2 and 3, the proportionality constant $D\infty$ can be calculated from $\Delta m_a = \Delta d \cdot \rho_f$ as

$$D_\infty = \frac{\rho_q N_q}{f^2}, \tag{4}$$

which for a quartz density of 2.65 g/cm^3 results in $D\infty = 12.28$ ng/(cm^2·Hz). This value refers to a situation where the deposition or removal of material is uniformly distributed over the entire quartz surface. If only a section of the surface is influenced by the ion bombardment, the spatial sensitivity of the induced frequency change becomes important. It is well known that the latter is described in good approximation by a Gaussian [35], [36]

$$\Delta f = \Delta f_0 \exp\left(-a\frac{r^2}{r_0^2}\right), \tag{5}$$

where r is the distance from the center of the quartz surface and r_0 is the radius of the bottom electrode deposited on the quartz crystal (3.3 mm).

To determine the shape constant a for the quartz crystal used here, we have measured the removal rate

for different values of r by translating the sample under the impinging ion beam. The C_{60}^+ ion beam is rastered across an area of about 100×100 μm^2. A typical result is shown in Figure 1. From the least square fit of eq 5 to the measured data (solid curves), we obtain a value of $a = 9.7$.

If only a fraction of the quartz crystal surface is exposed to the impinging primary ion beam, the proportionality constant D in eq 2 varies. Assuming, for simplicity, a radially symmetric beam profile of radius R centered on the surface, the resulting value D_R is determined by [36]

$$D_R = D_\infty \left[1 - \exp\left(-a\frac{R^2}{r_0^2} \right) \right]^{-1} \quad (6)$$

To determine the yield, we are interested in the total mass loss Δm instead of changes in the areal mass density $\Delta m_a = \Delta m / \pi R^2$. Combining eqs 2, 3, and 6, we obtain

$$\Delta m = \Delta d \cdot \rho_f \cdot \frac{\pi R^2}{1 - \exp\left(-a\frac{R^2}{r_0^2} \right)}. \quad (7)$$

If the exposed surface area is kept small enough to ensure that $aR^2/r_0^2 \leq 1$, eq 7 results in

$$\Delta m \cong \Delta d \cdot \rho_f \cdot \frac{\pi r_0^2}{a}, \quad (8)$$

where Δd is the removed layer thickness displayed by the QCM controller and ρ_f is the set film density value. The quantity $\pi r_0^2/a$ depicts the sensitive surface area of the quartz crystal which in our case has a diameter of ~ 2 mm. The removal rate displayed by the QCM controller is therefore independent of the ion beam raster area as long as (1) the total ion current delivered to the surface remains constant, (2) the raster area is centered on the crystal, and (3) the dimension of the exposed surface area does not exceed ~2 mm.

The resulting mass removal rate is then related to the flux of primary ions determined from the measured primary ion current. To obtain accurate results, the primary ion current must be corrected for ion bombardment-induced emission of charged secondary particles (ions and electrons) and is therefore independently measured using a Faraday cup. The total sputter yield is evaluated as the total number of atoms removed per impinging primary ion according to

$$Y_{tot} = \frac{\Delta m}{\Delta t} \cdot \frac{e \cdot N_A}{I_p \cdot m} = \frac{\Delta d}{\Delta t} \cdot \rho_f \cdot \frac{\pi r_0^2}{a} \cdot \frac{e N_A}{I_p m}, \quad (9)$$

where $\Delta d/\Delta t$ denotes the removal rate displayed by the QCM controller, e is the elementary charge, N_A is
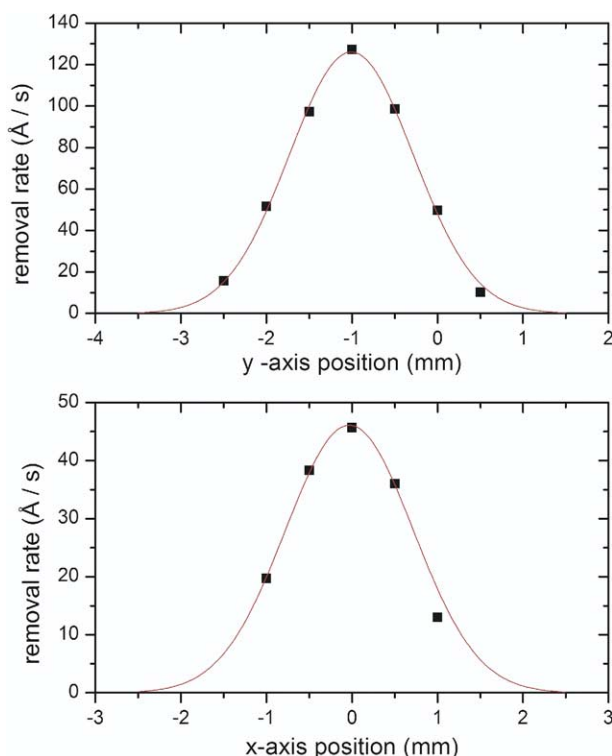

Figure 1. Lateral dependence of the removal rate measured on a 500 nm silver film deposited on a quartz crystal bombarded by 20-keV C_{60}^+ ions. The projectile ion beam was rastered across a surface area of 100×100 μm^2. The solid curve displays a Gaussian least square fit to the measured data.

Avogadro's number, m is the atomic mass of the target material (here: silver) and I_p is the primary ion current.

Results and Discussion

Total yield

The total number of silver atoms released per C_{60}^+ projectile impact onto the polycrystalline Ag surface with kinetic energies of 10, 15, and 20 keV is depicted in Table 1. For comparison, corresponding data measured under bombardment with 15-keV Ga^+ is also included. It is seen that the yield induced by 15-keV C_{60}^+ is about 5-fold higher than that induced by Ga^+ projectiles of the same impact energy. The yield measured under C_{60}^+ bombardment is found to depend linearly (R^2 of 0.9991) on the impact energy. At 20 keV, about 150 Ag atoms are released per C_{60} projectile, a value which is significantly larger than those typically achievable with atomic projectiles.

For comparison with recent MD computer simulations performed for the same projectiles impinging onto a (111) surface of an ideal Ag single crystal [21], the MD data have been included in Table 1. First, it is seen that the measured yield variations are in qualitative agreement with the simulation. This is particularly true for the impact energy dependence observed under C_{60} bombardment, where the experiment detects almost

Table 1. Total sputter yield of a polycrystalline Ag film deposited onto a quartz crystal under bombardment with C_{60}^+ and Ga^+ ions, respectively

		10-keV C_{60}^+	15-keV C_{60}^+	20-keV C_{60}^+	15-keV Ga^+
Experiment	absolute	47	98	144	20
	relative	1	2.1	3.1	0.42
MD Simulation	absolute	174	327 (0°)	482	21
	relative	1	1.9	2.8	0.12

The projectiles impinge onto the surface under an angle of 40 degrees with respect to the surface normal. Absolute values are given in atoms/projectile. For comparison, data obtained from molecular dynamics simulations [21] of neutral C_{60} and Ga impact onto a (111) single crystal Ag surface have been included. The accuracy of the experimental data is estimated to be of the order of $\pm$ 10%, the statistical uncertainty of the MD results is between 10 and 20%.

identical ratios as predicted from the simulations [22]. Comparing the absolute yield values, we find the experimental C_{60} data to be about a factor of 3 lower than predicted, whereas the value measured for Ga is almost exactly reproduced by the simulation.

The observed difference between measured and calculated yields of Ag after C_{60}^+ bombardment is not unexpected. The experiments were performed at an angle of incidence of 40° with respect to the surface normal while the calculations were performed at normal incidence. As shown in Table 1, the yield is expected to be smaller for off-normal angles. Moreover, there is preliminary XPS evidence [37] and results from MD simulations [21] that suggest there is ~5% carbon incorporation into the surface region. This modification would have an unknown effect on the measured yield. Finally, we expect that intrinsic surface roughness associated with the evaporated Ag film will produce a lower yield than the perfectly flat {111} surface. For example, yield measurements from an Ag film deposited on a roughened Au QCM target (data not shown) were about 50% lower than those found for Ag deposited on a smooth Au QCM target (Table 1). Some of these experimental uncertainties also apply to the Ga yield measurements, and we therefore view the close agreement between calculation and experiment in this case to be fortuitous. Hence, although there is uncertainty in the absolute sputtering yield, we believe the relative values reported in Table 1 as a function of incident energy are reliable.

Partial Yields

The partial yields of Ag atoms and Ag_n clusters are investigated using laser postionization of the respective sputtered neutral particles. More specifically, the average number of neutral species X desorbed per projectile impact is given by

$$Y(X^0) = Y_X \cdot (1 - \alpha_X^+ - \alpha_X^-), \qquad (10)$$

where $a_X^{+, -}$ denotes the probability that the particle is emitted as a positive or negative secondary ion, respectively. For a clean Ag surface bombarded with various atomic projectile ions, it has been established [38–42] that these ionization probabilities are small compared

to unity, thus making the neutral yield representative of the partial yield Y_X. If postionization conditions such as laser geometry and intensity are kept constant, the signal of a particular postionized species can be taken to represent the behavior of the partial yield of that species upon impact of different projectiles with different kinetic energies.

Laser postionization mass spectra of a polycrystalline Ag surface bombarded with 15 keV Ga^+ and 10, 15, and 20 keV C_{60}^+ ions are shown in Figure 2. The vertical axis representing the signal intensity is plotted in arbitrary units which correspond to the digitized MCP output. To compare the partial yields of the different ejected species, the spectra have been normalized to the primary ion current, which is different depending upon
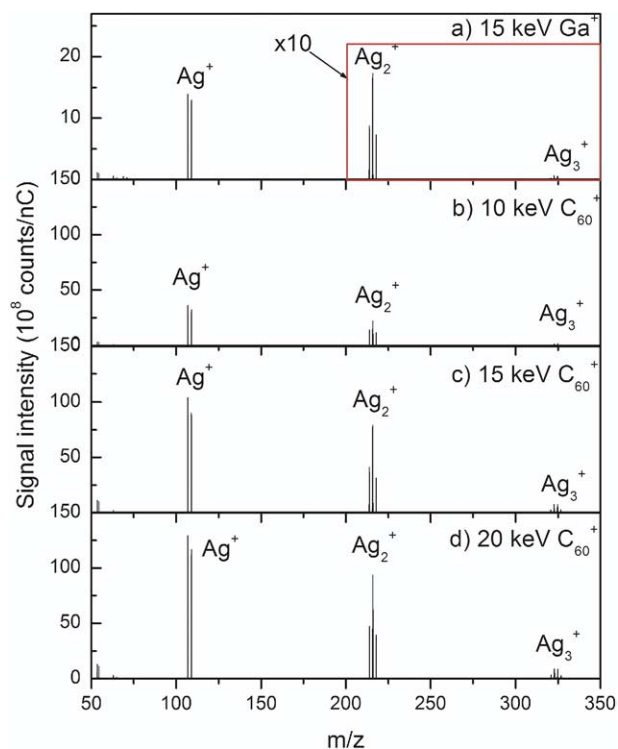

Figure 2. Laser postionization spectra of neutral Ag atoms and clusters produced by (**a**) 15 keV Ga^+ and (**b**), (**c**), (**d**) 10, 15, and 20 keV C_{60}^+. The laser pulses used are 800 nm pulses at a peak power density of 3.0 × 10^{12} W/cm². The signal intensity has been normalized to the primary ion current.

the projectile and impact kinetic energy. In all four cases, neutral Ag, Ag_2, and Ag_3 particles are readily observed. In accordance with published literature data [41, 43], the cluster intensities are found to decrease by roughly one order of magnitude with each additional Ag atom. Note, however, that the postionization probabilities of the different species are largely unknown, and the depicted intensities may not correctly reflect the yield ratio between different ejected species. The data are nevertheless useful to determine the yield variation of one particular species upon changing between different projectiles and impact kinetic energies.

From Figure 2, it is obvious that the Ag monomer neutral yields from C_{60}^+ bombardment are significantly larger than those from Ga^+ bombardment and increase with increasing impact kinetic energy. This finding is expected in view of the total yield changes determined above. To quantitatively compare the enhancements, we examine relative changes in the Ag_n neutral and secondary ion yields obtained under C_{60}^+ bombardment compared with those obtained under 15 keV Ga^+ bombardment. More specifically, the respective peaks in the TOF mass spectra are integrated over the entire isotopic abundance pattern, normalized to the primary ion current, and the ratio between the data obtained from C_{60}^+ and Ga^+ bombardment is calculated as an enhancement factor. The results are listed in Table 2 for 10, 15, and 20 keV impact energy. For comparison, the respective data obtained from the MD simulations [22] are also presented. As can be seen from the table, we find a qualitative agreement between the measured data and the prediction from the simulations. For instance, a 5.6-fold enhancement is measured for neutral Ag monomers between 15 keV C_{60}^+ and Ga^+ bombardment, whereas the predicted partial yield enhancement is 7-fold. Note that this value is also in very good agreement with the variation of the total sputter yield between 15 keV C_{60}^+ and 15 keV Ga^+ bombardment (Table 1), verifying that the majority of the desorbed material is ejected in the form of neutral monomers.

The enhancements are more pronounced for ejected dimers and trimers, a finding which also agrees with the simulation results. The fact that the measured yield enhancement appears to be consistently smaller than that predicted by the simulation may in part be attributed to the relatively large statistical error of the simulated multimer yields (particularly for Ga^+ projectiles). On the other hand, it may also relate to the fact that the experiment detects only a narrow solid angle interval centered around the surface normal, while—again for statistical reasons—the simulation data refer to all ejected particles regardless of emission angle. The observed differences would therefore indicate a more forward-peaked angular distribution of sputtered multimers for Ga^+ than for C_{60}^+ projectiles. Now, the statistics of the simulations are not sufficient to allow a more elaborate discussion of that point.

An important observation in Table 2 is that the yield variations measured for neutral Ag_n species are almost identical to those obtained for Ag_n^+ secondary ions. This finding indicates that the ionization probability a^+ of sputtered atoms and clusters is not significantly (i.e., by more than a factor of two) changed by the transition from Ga^+ to C_{60}^+ projectiles. The observed enhancements are therefore predominantly caused by a more efficient sputter removal of material which reflects both in increased total and partial sputtering yields obtained under C_{60}^+ cluster ion bombardment. This finding con-

Table 2. Partial sputtering yield ratio of Ag_n^+ secondary ions and Ag_n secondary neutral particles emitted from a polycrystalline silver surface under irradiation with 10, 15, and 20 keV C_{60}^+ and 15 keV Ga^+ bombardment

10 keV		Enhancement factor ($Y_{C_{60}^+}/Y_{Ga}^+$)		
		Ag	Ag_2	Ag_3
Experiment (40° incidence)	SIMS	0.7	3.5	11.9
	Laser Postionization	2.0	2.7	5.1
MD Simulation (normal incidence)		4.4	14	7
15 keV		Enhancement factor ($Y_{C_{60}^+}/Y_{Ga}^+$)		
		Ag	Ag_2	Ag_3
Experiment (40° incidence)	SIMS	3.8	10.5	25.1
	Laser Postionization	5.6	9.1	23.5
MD Simulation (normal incidence)		7	28	40
20 keV		Enhancement factor ($Y_{C_{60}^+}/Y_{Ga}^+$)		
		Ag	Ag_2	Ag_3
Experiment (40° incidence)	SIMS	4.5	18.9	48.7
	Laser Postionization	7.9	10.6	28.5
MD Simulation (normal incidence)		11	39	57

For comparison, data obtained from molecular dynamics simulations [21] of neutral C_{60} and Ga normally incident onto a (111) single crystal silver surface have been included. The uncertainty of the reported values is estimated to be of the order of 10% for monomers, increasing to about a factor two for trimers.

trasts with the results of a similar study performed for SF_5^+ projectile ions [18], where the yield enhancement of Ag_n^+ secondary ions was found to be almost entirely atributable to an increased ionization probability. Apparently, the effect of the polyatomic nature of the projectile ion impinging onto an Ag surface is large for C_{60}^+ but smaller for SF_5^+ projectile ions.

Velocity Spectra

The velocity distributions of neutral particles are derived from their flight time between the sample surface and the laser postionization volume. The measured flight time distributions of Ag and Ag_2 emitted by bombardment with (Figure 3a) 15-keV Ga^+, (Figure 3b) 10-keV C_{60}^+, (Figure 3c) 15-keV C_{60}^+, and (Figure 3d) 20-keV C_{60}^+ projectile ions are displayed in Figure 3. The data have been integrated over the entire isotope abundance distribution in the mass spectra. Due to the geometric setup, the distributions contain neutral species desorbing from the target over a wide polar angle interval extending up to $\pm30°$.

It is obvious that pronounced differences are found between atomic and cluster bombardment. Converting the data into emission velocity distributions by means of eq 1, we obtain the results displayed in Figure 4. The corresponding kinetic energy distributions are shown
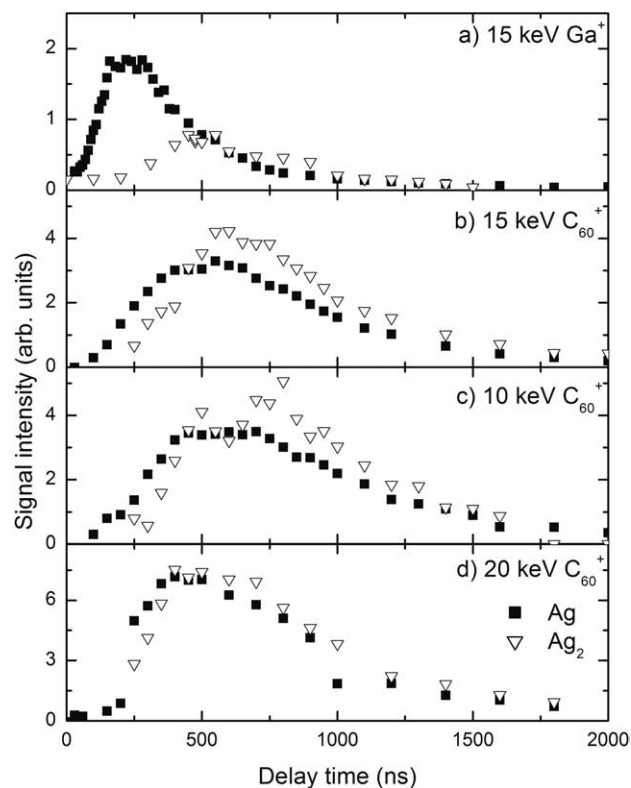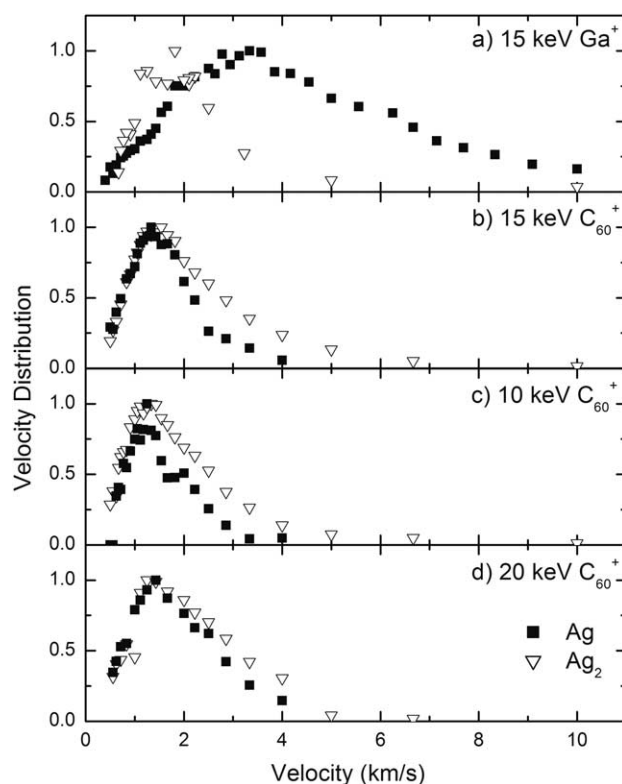

Figure 4. Emission velocity distributions of neutral Ag atoms and Ag_2 dimers emitted from a polycrystalline Ag surface under (**a**) 15 keV Ga^+, (**b**) 15 keV C_{60}^+, (**c**) 10 keV C_{60}^+, and (**d**) 20 keV C_{60}^+ bombardment.

in Figure 5. There are several interesting observations. The energy distributions of neutral Ag monomers induced by C_{60}^+ bombardment peak at lower values than those observed under Ga^+ bombardment. A similar shift towards lower kinetic energies under cluster impact has been reported earlier [20, 44], and is well reproduced by the MD simulation [21, 22]. This effect is qualitatively predicted by a simple thermal spike model of nonlinear sputtering, originally published by Sigmund and Claussen [45]. However, the experimental data cannot be fitted to the prediction of reference [45], shown, for instance, as a solid line in Figure 5d). Note that all kinetic energy distributions obtained under C_{60}^+ impact appear to be similar, indicating that the ejection process is largely independent of the primary ion impact energy.

Probably the most interesting observation in Figure 5 concerns the emission energy spectrum of sputtered Ag_2. It is seen that the most probable kinetic energy is *higher* than that of Ag. This finding is in pronounced contrast to the atomic projectile case, where the energy distributions of sputtered clusters peak at a lower emission energy than those of the monomers [41, 46–50]. Since the effect is found both in the experiments and in the MD simulations, it appears to represent a unique, new feature of the sputtering processes initiated by cluster impact.

To elucidate the cause of the observed differences,

Figure 3. Flight time distributions of neutral Ag atoms and Ag_2 dimers between the target surface and the postionization volume. The particles are desorbed from a polycrystalline Ag surface under (**a**) 15 keV Ga^+, (**b**) 15 keV C_{60}^+, (**c**) 10 keV C_{60}^+, and (**d**) 20 keV C_{60}^+ bombardment.
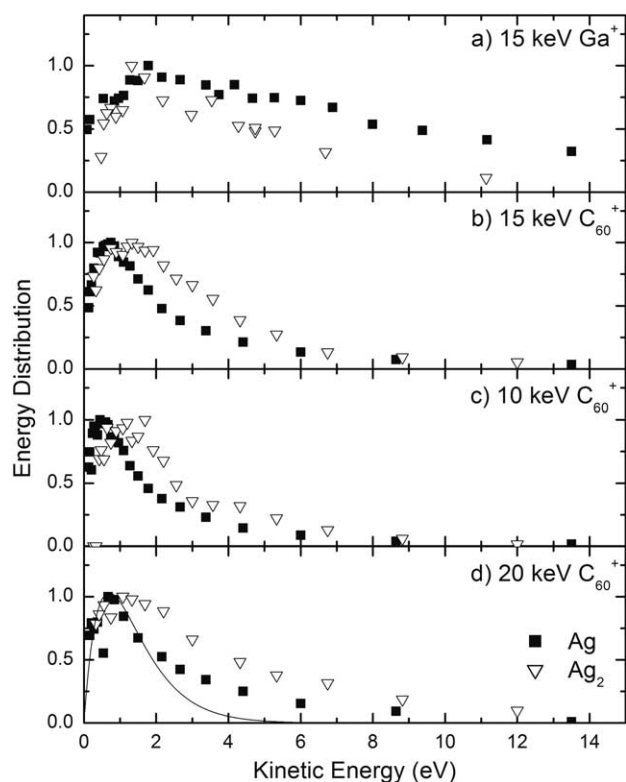
Figure 5. Emission energy distributions of neutral Ag and Ag_2 emitted from a polycrystalline silver surface under (**a**) 15 keV Ga^+, (**b**) 15 keV C_{60}^+, (**c**) 10 keV C_{60}^+, and (**d**) 20 keV C_{60}^+ bombardment. The solid curve in (**d**) depicts a Maxwell-Boltzmann energy distribution at T ~8000 K.

we return to the data displayed in Figure 4. Here, it is seen that the emission *velocity* distributions of Ag and Ag_2 observed under C_{60}^+ bombardment are surprisingly similar. A similar observation has been reported recently for the emission of In and In_2 from an In surface bombarded with Au atoms and clusters [19]. As discussed in reference [19], the situation under cluster projectile bombardment appears to resemble the case of an adiabatic gas expansion from a pressurized volume through a nozzle. In this scenario, all emitted particles would have the same velocity, regardless of their mass. The particle ejection mechanism might then be viewed as a jet-like expansion of a super-heated and super-dense gas being formed in the volume of the cascade induced by C_{60} impact. Due to the large pressure built up in the core of the impact zone, the surface is disrupted and material starts to expand quasi-freely into the vacuum. In fact, a similar picture has been used by Urbassek et al. [51, 52] describing the particle emission in spikes induced by keV-atom bombardment of condensed rare gases. By analyzing the emission velocity field in the cascade volume and in the vicinity of the surface, their simulations clearly demonstrate a correlated, jet-like motion of ejected particles which would be consistent with a gas flow model [53] of the ejection process. Comparing their visualization of impact events

induced by 1-keV Ar impinging onto solid Ar (Figures 1 and 5 in reference [52] and [51], respectively) with those induced by 15-keV C_{60} impinging onto Ag{111} (Figures 2 and 1 in references [22] and [21], respectively), it is probable that the nature of the emission mechanism must be similar in both cases. This notion is consistent with the fact that the kinetic energy spectrum of emitted atoms peaks at lower energies than predicted by linear cascade theory, but on the other hand cannot be fitted to a simple Maxwellian distribution.

Conclusions

Our results show that if C_{60}^+ projectiles are used to bombard a metal surface instead of isoenergetic Ga^+ ions, the yields of sputtered neutral species are enhanced by about the same amount as those of secondary ions. Moreover, the measured total sputter yield exhibits similar enhancement to that of sputtered neutral monomers. As a consequence, the secondary ion signal enhancement must be caused by a more efficient particle emission process rather than by a more efficient ionization of the ejected species. Moreover, neutral cluster species experience more enhancement than their corresponding monomers in a fashion also found for the secondary ions. The experimental results show that the neutral Ag species produced by C_{60}^+ bombardment leave the surface with kinetic energy distributions that maximize at much lower values than those observed under Ga^+ bombardment. In pronounced contrast to published data for atomic ion bombardment, we find that under C_{60} impact the emission *velocity* distributions of sputtered monomers and clusters are nearly identical.

The experimental findings are in at least qualitative agreement with recent MD simulations of the emission kinetics induced by C_{60} and Ga impact onto an Ag{111} surface. In total, the data indicate that the particle emission mechanism induced by the cluster projectile impact is significantly different from linear cascade sputtering typically encountered for atomic projectiles. Evaporation from thermal spikes, on the other hand, would lead to similar kinetic *energy* distributions of the emitted monomers and dimers and can therefore be ruled out as the predominant mechanism. The data seem best to be described by a jet expansion mechanism where a superheated, gasified volume of material in the core of the collision cascade builds up enough pressure to disrupt the surface and expand quasi-freely into the vacuum.

Acknowledgments

References

1. Castner, D. G. Surface science—View from the edge. *Nature* **2003**, *422*, 129–130.
2. Winograd, N. The magic of cluster SIMS. *Anal. Chem.* **2005,** *77*, 142A–149A.
3. Weibel, D.; Wong, S.; Lockyer, N.; Blenkinsopp, P.; Hill, R.; Vickerman, J. C. A C_{60} primary ion beam system for time of flight secondary ion mass spectrometry: Its development and secondary ion yield characteristics. *Anal. Chem.* **2003**, *75*, 1754–1764.
4. Wong, S. C.; Hill, R.; Blenkinsopp, P.; Lockyer, N. P.; Weibel, D. E; Vickerman, J. C. Development of a C-60(+) ion gun for static SIMS and chemical imaging. *Appl. Surf. Sci.* **2003**, *203*, 219–222.
5. Davies, N.; Weibel, D.E.; Blenkinsopp, P.; Lockyer, N.; Hill, R.; Vickerman, J.C. Development and experimental application of a gold liquid metal ion source. *Appl. Surf. Sci.* **2003**, *203*, 223–227.
6. Kersting, R.; Hagenhoff, B.; Kollmer, F.; Mollers, R.; Niehuis, E. Influence of primary ion bombardment conditions on the emission of molecular secondary ions. *Appl. Surf. Sci.* **2004**, *231/232*, 261–264.
7. Cornett, D. S.; Lee, T. D.; Mahoney, J. F. Matrix-free desorption of biomolecules using massive cluster-impact. *Rapid Commun. Mass Spectrom.* **1994**, *8*, 996–1000.
8. Wagner, M. S. Impact energy dependence of SF5± induced damage in poly(methyl methacrylate) studied using time-of-flight secondary ion mass spectrometry. *Anal. Chem.* **2004**, *76*, 1264–1272.
9. Mahoney, C. M.; Roberson, S.; Gillen, G. Depth profiling of 4-acetamindophenol-doped poly(lactic acid) films using cluster secondary ion mass spectrometry. *Anal. Chem.* **2004**, *76*, 3199–3207.
10. Gillen, G.; Fahey, A. Secondary ion mass spectrometry using cluster primary ion beams. *Appl. Surf. Sci.* **2003**, *203/204*, 209–213.
11. Wucher, A.; Sun, S.; Szakal, C.; Winograd, N. Molecular depth profiling of histamine in ice using a buckminsterfullerene probe. *Anal. Chem.* **2004**, *76*, 7234–7242.
12. Sostarecz, A. G.; Sun, S.; Szakal, C.; Wucher, A.; Winograd, N. Depth profiling studies of multilayer films with a C60+ ion source. *Appl. Surf. Sci.* **2004**, *231/232*, 179–182.
13. Sun, S.; Wucher, A.; Szakal, C.; Winograd, N. Depth profiling of polycrystalline multilayers using a buckminsterfullerene projectile. *Appl. Phys. Lett.* **2004**, *84*, 5177–5179.
14. Sun, S.; Szakal, C.; Roll, T.; Mazarov, P.; Wucher, A.; Winograd, N. The use of C_{60} cluster projectiles for sputter depth profiling of polycrystalline metals. *Surf. Interface Anal.* **2004**, *36*, 1367–1372.
15. Wucher, A.; Sun, S.; Szakal, C.; Winograd, N. Molecular depth profiling in ice matrices using C_{60} projectiles. *Appl. Surf. Sci.* **2004**, *231/232*, 68–71.
16. Szakal, C.; Sun, S.; Wucher, A.; Winograd, N. C_{60} molecular depth profiling of a model polymer. *Appl. Surf. Sci.* **2004**, *231/232*, 183–185.
17. Sostarecz, A. G.; McQuaw, C. M.; Wucher, A.; Winograd, N. Depth profiling of Langmuir-Blodgett films with a buckminsterfullerene probe. *Anal. Chem.* **2004**, *76*, 6651–6658.
18. Ghalab, S.; Staudt, C.; Maksimov, S. E.; Mazarov, P.; Tugushev, V. I.; Dzhemilev, N. K.; Wucher, A. Formation of sputtered silver clusters under bombardment with SF$_{5+}$ ions. *Nucl. Instrum. Methods B.* **2002**, *197*, 43–48.
19. Samartsev, A. V., Wucher, A. Sputtering of indium using Au$_m$ projectiles: Transition from linear cascade to spike regime; unpublished.
20. Andersen, H. H. Nonlinear effects in collisional sputtering under cluster impact. In *Fundamental processes in sputtering of atoms and molecules (SPUT 92)*, 43 ed.; Sigmund, P., Ed.; Det Kongelige Danske Videnskabernes Selskab: Copenhagen, 1993; p 127.
21. Postawa, Z.; Czerwinsky, B.; Szewczyk, M.; Smiley, E. J.; Winograd, N.; Garrison, B. J. Microscopic insights into the sputtering of Ag{111} induced by C60 and Ga bombardment. *J. Phys. Chem. B.***2004**, *1*, 7831–7837.
22. Postawa, Z.; Czerwinski, B.; Szewczyk, M.; Smiley, E. J.; Winograd, N.; Garrison, B. J. Enhancement of sputtering yields due to C-60 versus Ga bombardment of Ag{111} as explored by molecular dynamics simulations. *Anal. Chem.* **2003**, *75*, 4402–4407.
23. Kerford, M.; Webb, R. P. Molecular dynamics simulation of the desorption of molecules by energetic fullerene impacts on graphite and diamond surfaces. *Nucl. Instrum. Methods B*; **1999**, *153*, 270–274.
24. Aoki, T.; Seki, T.; Matsuo, J.; Insepov, Z.; Yamada, I. Molecular dynamics simulation of a carbon cluster ion impacting on a carbon surface. *Mater. Chem. Phys.* **1998**, *54*, 139–142.
25. Seki, T.; Aoki, T.; Tanomura, M.; Matsuo, J.; Yamada, I. Energy dependence of a single trace created by C-60 ion impact. *Mater. Chem. Phys.* **1998**, *54*, 143–146.
26. Aderjan, R.; Urbassek, H. M. Molecular-dynamics study of craters formed by energetic Cu cluster impact on Cu. *Nucl. Instrum. Methods B* **2000**, *164/165*, 697–704.
27. Webb, R.; Kerford, M.; Way, A.; Wilson, I. Comparison of gold and carbon cluster impacts on graphite using molecular dynamics simulation. *Nucl. Instrum. Methods B* **1999**, *153*, 284–291.
28. Braun, R. M.; Blenkinsopp, P.; Mullock, S. J.; Corlett, C.; Willey, K. F.; Vickerman, J. C.; Winograd, N. Performance characteristics of a chemical imaging time-of-flight mass spectrometer. *Rapid Commun. Mass Spectrom.* **1998,** *12*, 1246–1252.
29. Matt, S.; Dunser, M.; Lezius, M.; Deutsch, H.; Becker, K.; Stamatovic, A.; Scheier, P.; Mark, T. D. Absolute partial and total cross-section functions for the electron impact ionization of C-60 and C-70. *J. Chem. Phys.* **1996**, *105*, 1880–1896.
30. Brummel, C. L.; Willey, K. F.; Vickerman, J. C.; Winograd, N. Ion beam induced desorption with postionization using high repetition femtosecond lasers. *Int. J. Mass Spectrom. Ion Processes* **1995**, *143*, 257–270.
31. Willey, K. F.; Brummel, C. L.; Winograd, N. Photoionization mechanisms for Cr(CO)$_6$ using high intensity laser pulses in the near-IR. *Chem. Phys. Lett.* **1997**, *267*, 359–364.
32. Wucher, A.; Wahl, M.; Oechsner, H. Sputtered neutral silver clusters up to Ag$_{18}$. *Nucl. Instrum. Methods B* **1993**, *82*, 337–346.
33. Sauerbrey, G. *Zeitschrift für Physikalische Chemie.* **1959**, *155*, 206–222.
34. Kanazawa, K. K.; Melroy, O. R. The quartz resonator: Electrochemical applications. *IBM J. Res. Dev.* **1993**, *37*, 157–171.
35. Martin, B. A.; Hager, H. E. Velocity profile on quartz crystals oscillating in liquids. *J. Appl. Phys.* **1989**, *65*, 2630–2635.
36. Doemling, M. F.; Lin, B.; Rueger, N. R.; Oehrlein, G. S.; Haring, R.; Lee, Y. H. Using a quartz crystal microbalance for low energy ion beam etching studies. *J. Vac. Sci. Technol. A* **2000**, *18*, 232–236.
37. Preliminary data acquired by ULVAC-PHI Inc. using 10-keV C60+ projectiles; http://www.phi.com
38. Yu, M. L. Charged and excited states of sputtered atoms. In *Sputtering by particle bombardment, III*; Behrisch, R.; Wittmaack, K., Eds.; Springer: Berlin, 1991; p 91.
39. Meyer, S.; Staudt, C.; Wucher, A. Ionization probability of atoms and molecules sputtered from a cesium covered silver surface. *Appl. Surf. Sci.* **2003**, *203–204*, 48–51.
40. Wucher, A; Heinrich, R; Staudt, C. A method for quantitative determination of secondary ion formation probabilities. In *Secondary ion mass spectrometry (SIMS XII)*; Benninghoven, A.;

Bertrand, P.; Migeon, N.; Werner, H.W., Eds.; Elsevier Science: Amsterdam, 2000; p 143.

41. Wahl, M.; Wucher, A. VUV photoionization of sputtered neutral silver clusters. *Nucl. Instrum. Methods B* **1994**, *94*, 36–46.

42. Wucher, A.; Berthold, W.; Oechsner, H. In *The charge state of sputtered metal clusters*; Benninghoven, A.; Nihei, Y.; Shimizu, R.; Werner, H. W.; Eds.; Wiley and Sons: 1994; p 100.

43. Franzreb, K.; Fine, J. The significance of autoionization processes during nonresonant one-color two-photon ionization of neutral silver and copper atoms at $\lambda = 248$ nm. *Nucl. Instrum. Methods B* **1993**, *83*, 266–274.

44. Szymonski, M.; Bhattacharya, R. S.; Overeijnder, H.; de Vries, A. E. Sputtering of an AgAu alloy by bombardment with 6 keV Xe^+ ions. *J. Phys. D* **1978**, *11*, 751–759.

45. Sigmund, P.; Claussen, C. Sputtering from elastic-collision spikes in heavy-ion-bombarded metals. *J. Appl. Phys.* **1981**, *52*, 990–993.

46. Bernhardt, F.; Oechsner, H.; Stumpe, E. Energy distributions of neutral atoms and molecules sputtered from polycrystalline silver. *Nucl. Instrum. Methods B* **1976**, *132*, 329–334.

47. Dembowski, J.; Oechsner, H.; Yamamura, Y.; Urbassek, H. M. Energy distributions of neutral atoms sputtered from Cu, V, and Nb under different bombardment and ejection angles. *Nucl. Instrum. Methods B* **1987**, *18*, 464–470.

48. Brizzolara, R. A.; Cooper, C. B. Measurements of energy distributions and yields of neutral Cu_2 and Cu_3 species sputtered from Cu by low energy Ar^+ ions. *Nucl. Instrum. Methods B* **1989**, *43*, 136–145.

49. Cooper, C. B.; Hamed, H. A. Experiments on the sputtering of neutral Cu_2 dimers from Cu by Ar^+ ions (60–300 eV). *Surf. Sci.* **1984**, *143*, 215–222.

50. Coon, S. R.; Calaway, W. F.; Burnett, J. W.; Pellin, M. J.; Gruen, D. M.; Spiegel, D. R.; White, J. M. Yields and kinetic energy distributions of sputtered neutral copper clusters. *Surf. Sci.* **1991**, *259*, 275–287.

51. Waldeer, K. T.; Urbassek, H. M. keV-Atom bombardment of condensed rate gases: Molecular dynamics simulation. *Nucl. Instrum. Methods B* **1993**, *73*, 14–28.

52. Urbassek, H. M.; Waldeer, K. T. Spikes in condensed rate gases induced by keV-atom bombardment. *Phys. Rev. Lett.* **1991**, *67*, 105–108.

53. Urbassek, H. M. On rovibrational excitation in the sputtering of molecules: A quantum mechanical description. *J. Phys. B* **1987**, *20*, 3105–3123.